PERGAMON

International Journal of Heat and Mass Transfer 44 (2001) 3201–3211

International Journal of HEAT and MASS TRANSFER

www.elsevier.com/locate/ijhmt

Theoretical and experimental analysis of droplet diameter, temperature, and evaporation rate evolution in cryogenic sprays

G. Aguilar [a,b,*], B. Majaron [b,d], W. Verkruysse [b], Y. Zhou [c], J.S. Nelson [a,b], E.J. Lavernia [c]

[a] *Whitaker Center for Biomedical Engineering, University of California, Irvine, CA 92697, USA*
[b] *Beckman Laser Institute and Medical Clinic, University of California, Irvine, CA 92612, USA*
[c] *Department of Chemical and Biochemical Engineering and Materials Sciences, University of California, Irvine, CA 92697, USA*
[d] *Jožef Stefan Institute, Jamova 39, SI-1000 Ljubljana, Slovenia*

Received 27 June 2000; received in revised form 17 November 2000

Abstract

Cryogenic sprays are used for cooling human skin during selected laser treatments in dermatology. In order to optimize their cooling efficiency, a detailed characterization and understanding of cryogen spray formation is required. Various instruments and procedures are used to obtain mean size (D), velocity (V), and temperature (T) of tetrafluoroethane spray droplets from straight-tube nozzles. A single-droplet evaporation model is used to predict droplet diameter and temperature as a function of distance from the nozzle, $D(z)$ and $T(z)$, from the values of D, V, and T at the nozzle exit, i.e., D_0, V_0, and T_0. In the model, it is assumed that D and V decrease in accordance with the D^2-law, and due to drag force, respectively. To compute $T(z)$, the instantaneous D and V are incorporated into a phase-change heat transfer balance, which includes a heat convection term. The predicted evolutions of $T(z)$ and $D(z)$ are in reasonable agreement with experimental data.

Keywords: Atomization; Coalescence; Heat transfer; Nozzle; Spray cooling

1. Introduction

Cryogenic sprays are of interest in selected medical applications, e.g., for cooling of human skin during laser treatment of port wine stain birthmarks (PWS) [1,2] and hair removal [3]. Patients are treated with laser pulses that induce permanent thermal damage to the targeted PWS blood vessels typically located 200–550 μm below the skin surface [4], or to hair follicles, which may be up to several millimeters deep [5]. However, absorption of laser energy by melanin causes localized heating of the superficial skin layer (epidermis), which may result in scarring or dyspigmentation [6]. By applying a cryogen spurt to the skin surface for an appropriately short period of time (typically 10–100 ms), the epidermis is cooled selectively prior to application of the laser pulse [7]. The objective of this precooling is to achieve the largest possible temperature difference between the epidermis and the deeper targeted vessels [8]. To achieve optimal cooling selectivity, it is necessary to precisely control the precooling time [9]. For that purpose, cryogen spray cooling (CSC) offers an ideal solution, and has been used in commercial dermatological devices for several years. Nevertheless, it is still necessary to design atomizing nozzles to provide a high heat extraction rate from the skin surface and, ideally, cover a sprayed area similar in size to that of the laser beam. To enhance the understanding of nozzle design, cryogen spray characteristics are needed, such as mean droplet size, velocity, temperature, and evaporation rates, and their relation to heat extraction rate from the skin surface.

* Corresponding author. Tel.: +1-949-824-3754; fax: +1-949-824-6969.
E-mail address: gaguilar@bli.uci.edu (G. Aguilar).

0017-9310/01/$ - see front matter
PII: S0017-9310(00)00363-X

Nomenclature

A	surface area
C_D	drag coefficient acting on droplet
C_f	friction coefficient acting on liquid flow
c	specific heat at constant pressure
D	droplet diameter
F_D	drag force
k	thermal conductivity
L	latent heat of vaporization
m	mass
M	molecular weight
Nu	Nusselt number
P	pressure
ΔP	pressure drop
Pr	Prandtl number
Q	thermal energy
Re	Reynolds number
T	average temperature
V	bulk or average velocity
z	distance from the nozzle

Greek symbols

ρ	density
λ	evaporation constant
μ	dynamic viscosity

Subscripts

a	air
d	relative to the droplet
g	relative to the air–cryogen vapor mixture
ℓ	liquid
N	relative to the nozzle
s	relative to the surface
∞	relative to ambient
0	initial
1	relative to time t_1

Superscript

$'$	subject to convective conditions

To date, there have been several studies on water sprays, from which empirical correlations of various spray characteristics have been developed. Harmon [10], Tanasawa and Toyoda [11], and Elkobt [12] proposed correlations to estimate the Sauter mean diameter (SMD) of droplets produced by plain orifice atomizers. However, these correlations do not account for liquid evaporation, which is likely to be significant in cryogenic sprays. Studies of droplet evaporation in liquid fuel sprays have led to development of a simple model, which takes into consideration the evaporation rate of droplets under quiescent conditions ($\delta m/\delta t$) [13]. Moreover, in order to account for the convective effects on droplets in motion relative to the surrounding air, a semi-empirical correlation proposed earlier by Ranz and Marshall [14] may be applied to this model to compute a corrected evaporation rate ($\delta m'/\delta t$).

Regarding cryogenic sprays, Ingebo [15–20] studied the effects of gas temperature, gas properties, and vaporization on droplet size of sprays produced by two-fluid type nozzles, where a high velocity gas was used to atomize the liquid cryogen. As a result, some correlations were proposed to predict mean droplet diameters of cryogen sprays based on the gas mass flux, cryogen and gas properties, and nozzle geometry. However, for two-fluid nozzles atomization takes place mostly by violent impingement of high velocity gas jet against a slowly moving liquid, whereas for single-fluid nozzles – as those used in this study – the atomization results from strong shear stresses acting in a liquid jet, as it is forced through small diameter nozzles (typically 0.5–2 mm). Therefore, the droplet diameter correlations developed for two-fluid nozzles may not be applicable to the present experimental conditions. More recently, Estes and Mudawar [21] studied the evaporation efficiency of water and Fluorinert (Fluorocarbon compounds used for vapor phase heating applications) sprays by measuring the heat flux across a sprayed surface and its variation with surface temperature and flow rate, for three nozzles. A product of this study was a correlation that predicts the heat flux based on nozzle geometry, fluid properties, spray droplet diameter, and volumetric flow.

The ultimate objective of the present investigation is to improve our understanding of cryogenic sprays for biomedical applications. First, Fast Flash Lamp Photography (FFLP) is used to analyze the general spray characteristics produced by two straight-tube nozzles of equal diameter (D_N) but different lengths (L_N); secondly, various techniques and instruments are implemented to obtain systematic measurements of mean droplet diameter (D), mean droplet velocity (V) and average droplet temperature (T); a Phase Doppler Interferometer (PDI) as well as an Ensemble Particle Concentration & Sizing apparatus (EPCS) are used to obtain measurements of D. PDI is also used to provide information on V. Thermocouple-based measuring devices are utilized to measure T; and finally, a recently developed steady-state heat transfer coefficient measurement procedure [22] is used to determine the heat transfer coefficient at the skin–cryogen interface (h_{cryo}). To this extent, studies are focused on determining the evolution of D and T with distance from the nozzle tip (z), and relate these evolutions to the evaporation rate ($\delta m'/\delta t$) of tetrafluoroethane (HFC-134a) sprays.

A single-droplet evaporation model involving the phase-change heat transfer analysis is developed to relate the evolution of fundamental spray variables, i.e., D, V, and T. The predicted evolutions $T(z)$ and $D(z)$ are matched with the experimental results. The values at the exit of the nozzle (i.e., D_0, V_0, and T_0), which serve as an input to the model, are obtained by using a combination of theoretical estimates, extrapolation of experimental trends, and fitting of the predicted dependencies to the experimental data. In this way, the model serves also as an indirect way to determine the evaporation rate ($\delta m'/\delta t$) of cryogenic sprays. Even though the described analysis is focused on the evaporation process that takes place downstream from the nozzle tip, possible evaporation within the nozzle is also analyzed (see Appendix A).

In summary, the main objectives pursued in this work are to: (i) experimentally determine $D(z)$ and $T(z)$ for two straight-tube nozzles of different length; (ii) develop a single-droplet convection–diffusion model and compare its predictions to experimental data and; (iii) by matching the model predictions to the experimental results, indirectly determine $\delta m'/\delta t$ in cryogenic sprays.

2. Experimental setups and procedures

2.1. Spray forming setup

Two straight-tube nozzles were constructed at the Beckman Laser Institute and Medical Clinic (BLIMC), University of California at Irvine (UCI). Their geometry resembles that of commercial nozzles used for CSC in conjunction with dermatological laser treatments. These two custom-made nozzles consist of a stainless steel tube of length L_N and inner diameter D_N and a copper body that fits tightly around an auto fuel injector, used to electronically control the spurt duration. Table 1 shows a sketch and dimensions of these two nozzles.

The cryogen is delivered through a standard high-pressure hose connecting the cryogen vessel to the fuel injector. The vessel is a commercial HFC-134a cryogen container, which is pressurized at the saturation pressure of this cryogen at room temperature (6.7 bar at 25°C). To avoid significant cryogen evaporation upstream of the nozzle, a hose with large diameter relative to the nozzle diameter is used and the cryogen vessel is positioned about 1 m above the nozzle.

2.2. Imaging setup

A progressive-scan CCD camera with shutter speed of 60 μs (9700 TMC by Pulnix, Sunnyvale, CA) is used to take photographs of the sprays produced by both nozzles. A flashlamp (FX-1160 by EG&G Electronics, Salem, MA) provides illumination gating by about 5 μs long pulses that "freeze" the image of flying cryogen droplets with a lateral resolution around 20 μm. The supporting electronics enable acquisition of image sequences at 30 frames per second with precisely controlled delays with respect to the onset of the cryogen spurt. The flashlamp and the camera are positioned in the same horizontal plane, with the camera viewing perpendicularly to the spray axis and all pictures are taken under equal lighting conditions. The sprays are photographed at two different magnifications. To obtain low magnification images, the camera is placed 470 mm from the nozzle tip, and the flashlamp directed towards the nozzle tip at a 30° angle with respect to the camera axis. With this arrangement it is possible to obtain a field of view of about 75×47 mm^2. For high magnification images, the camera is positioned approximately 130 mm from the nozzle tip, which results in a field of view of about 17×14 mm^2.

2.3. Droplet size and velocity measurements

An Ensemble Particle Concentration & Sizing apparatus (EPCS by Insitec/Malvern, Worcestershire, UK) is used to conduct systematic measurements of droplet diameter (D) as a function of z. The operation of this instrument is based on Fraunhofer diffraction of a parallel beam of monochromatic light (provided by a 670 nm diode laser) caused by the obstructing spray drop-

Table 1
Sketch of straight-tube nozzles configuration and dimensions

Nozzle	L_N (mm)	D_N (mm)	L_N/D_N
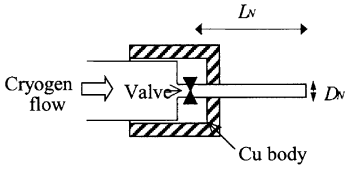			
Short (S)	31.8 (1.25 in)	1.4 (0.05 in)	23
Long (L)	63.5 (2.50 in)	1.4 (0.05 in)	46

lets. A more detailed description of this instrument can be found elsewhere [23]. In order to obtain more localized measurements, the laser beam is reduced from its normal diameter of 10 mm to about 3.3 mm with an inverted beam expander (OptoSigma, Santa Ana, CA). A positioning system is used to gradually displace the nozzles perpendicularly to the laser beam, from about 15 to 200 mm.

As a meaningful measurement of particle size, the Sauter mean diameter (SMD or D_{32}) is utilized. SMD represents the size of a droplet with the same surface area to volume ratio as that of the entire spray, and is known to characterize heat and mass transfer of the droplets better than the arithmetic mean diameter [23].

A PDI (Aerometrics, Sunnyvale, CA), utilized in our laboratory for metal spray characterization [24,25], was used to provide a couple of preliminary measurements of mean droplet size (D) and mean droplet velocity (V) close to the nozzle tip, where EPCS measurements become unreliable – most likely because of the high density spray. Although these measurements were performed on cryogenic sprays produced by a commercial nozzle (Scleroplus™ by Candela, Wayland, MA) with an inner diameter of about 0.8 mm (0.030″), they provide an important validation of the theoretical estimation of the initial droplet velocity V_0 (Section 3.2), which is then used for the two nozzles under study. It is also important to note that, while PDI measures the local values of D and V, EPCS represents an ensemble average, which better represents the whole spray.

2.4. Droplet temperature measurements

A type-K thermocouple with bead diameter of approximately 0.3 mm (5SC-TT-E-36 by Omega, Stamford, CT) is used to measure $T(z)$. The estimated response time of this kind of thermocouple is about 40 ms in still water at 100°C, and its ASTM standard wire error is below ±2.2°C for the range of temperatures measured. All spurts have durations of at least 1 s, which ensured steady state conditions for this thermocouple. The temperature sensor is supported by a rigid stick and inserted into the center of the spray cone at varying distances from the nozzle. The estimated uncertainty in z is ±0.5 mm. Since water condensation and freezing on the thermocouple bead can affect temperature measurements, these experiments are conducted in a chamber filled with dry air (relative humidity below 5%). Under such conditions, most of the tests do not show appreciable condensation, except for $z > 100$ mm, where signs of frost formation are observed around the thermocouple bead. Since at this point there is more interest in the general trend of $T(z)$ rather than tight-accuracy measurements, the uncertainties of T and z described above are acceptable.

3. Theoretical evaporation model

3.1. Droplet size (D) and evaporation rate ($\delta m'/\delta t$)

It is assumed that the decrease of a single droplet diameter as a function of time is given by the "D^2-law" [26]:

$$D^2 = D_0^2 - \lambda t, \tag{1}$$

where D_0 is the initial drop diameter and λ is the evaporation constant under quiescent conditions. The evaporation rate of a single droplet ($\delta m/\delta t$) can be expressed as

$$\frac{\delta m}{\delta t} = \frac{\pi}{2}\rho_\ell D^2 \frac{\partial D}{\partial t}, \tag{2}$$

where ρ_ℓ is the liquid cryogen density. Eq. (1) may be introduced into Eq. (2) to yield the evaporation rate of a single droplet under quiescent conditions:

$$\frac{\delta m}{\delta t} = \frac{\pi}{4}\rho_\ell \lambda D. \tag{3}$$

According to Ranz and Marshall [14], the evaporation rate of a single droplet subject to forced convection conditions ($\delta m'/\delta t$) is given by:

$$\frac{\delta m'}{\delta t} = 2\pi D\left(\frac{k_g}{c_g}\right)\ln(1+B_M)\left[1+0.3Re_d^{0.5}Pr_g^{0.33}\right], \tag{4}$$

where k_g, c_g, Re_d, and Pr_g are, respectively, the thermal conductivity, specific heat, and droplet Reynolds and Prandtl numbers relative to the air–cryogen vapor mixture surrounding the evaporating droplet. $B_M = Y_{\ell,s}/(1-Y_{\ell,s})$ is the mass transfer number, where $Y_{\ell,s}$ is the cryogen mass fraction at the droplet surface, defined as $Y_{\ell,s} = 1/[1+(1-P_\infty/P_{\ell,s})M_a/M_\ell]$ [23]. M_a, M_ℓ, P_∞ and $P_{\ell,s}$ are the air and cryogen molecular weights, and the ambient and cryogen vapor pressures at the droplet surface, respectively (see Table 2 for values). The term in the square brackets in Eq. (4) accounts for forced convection due to relative motion of the droplet with respect to its surroundings. Therefore, when forced convection at the droplet interface is considered, the corresponding convective evaporation rate, $\delta m'/\delta t$, can be expressed by a modified Eq. (3), where a convective evaporation constant, λ', replaces λ. By equating the modified Eq. (3) with Eq. (4), the convective evaporation constant (λ') may be expressed as:

$$\lambda' = \frac{8k_g\ln(1+B_M)}{c_g\rho_\ell}\left[1+0.3Re_d^{0.5}Pr_g^{0.33}\right]. \tag{5}$$

3.2. Droplet velocity (V)

In order to estimate the average droplet velocity at the nozzle exit (V_0), a single-phase turbulent flow of

Table 2
Properties of HFC-134a, air, and cryogen–air vapor mixture

k_g	0.017 W/(m K)
c_g	923 J/(kg K)
ρ_g	3.35 kg/m^3
μ_g	13.2×10^{-6} Pa s
P_∞	1.0 atm
$P_{\ell,s}$	6.7 atm
M_a	28.97 (kmol/kg)
M_ℓ	102.3 (kmol/kg)
ρ_ℓ	1294 kg/m^3
μ_ℓ	202×10^{-6} Pa s
Re_N	31,598
ρ_v	5.26 kg/m^3
μ_v	12×10^{-6} Pa s

liquid cryogen within the nozzle is assumed. Under such conditions, the bulk velocity within the nozzle can be expressed as:

$$V_0 = \sqrt{\frac{\Delta P D_N}{2\rho_\ell L_N C_f}}, \tag{6}$$

where ΔP, ρ_ℓ, and C_f are the total pressure drop between the cryogen tank and the atmosphere, liquid cryogen density, and friction coefficient, respectively. For simplicity, it is assumed that the whole ΔP takes place along the nozzle, i.e., the pressure drops along the hose and across the solenoid valve are neglected. The C_f for turbulent pipe flow can be expressed as: $C_f = 0.079 Re_N^{-0.25}$ (Blasius equation), to a reasonable degree of approximation. Here Re_N represents the Reynolds number for the flow within the nozzle: $Re_N = \rho_\ell V_0 D_N/\mu_\ell$; μ_ℓ being the liquid cryogen dynamic viscosity. For both nozzles, the total pressure drop (ΔP) is assumed to be 6.7 bar (≈97 psi), i.e., the relative pressure of the container. The density (ρ_ℓ) is estimated at 0°C (1294 kg/m^3), which is approximately the average between the cryogen container temperature (22–25°C), and the exit droplet temperature ($T_0 \approx -20$°C to −26°C), as shown below. For the dynamic viscosity (μ_ℓ), the reported value at 25°C is used (202×10^{-6} Pa s) [27].

To model the time evolution of the droplet velocity, it is assumed that deceleration is caused by the drag force (F_D) acting on a round sphere of surface area A, i.e., $F_D = 1/2\rho_g C_D V^2 A$, where ρ_g is the density of the gas surrounding the nozzle and C_D the drag coefficient. For the range of Re_d involved (50–450), a good approximation to the value of C_D is given by: $C_D = 5.8 Re_d^{-0.25}$. By incorporating this expression into the Newton's 2nd law, the instantaneous velocity of the sphere can be computed by successive iterations from the following equation:

$$V(t_1) = \frac{m_0 V_0 - \int_0^{t_1} F_D \, dt}{m(t_1)}. \tag{7}$$

3.3. Average droplet temperature (T)

To compute the average droplet temperature, an energy balance is established between the initial time, t_0, and a subsequent time, t_1, at which a part of the droplet has evaporated. Therefore

$$H_0 = H_{1,\ell} + (H_{1,g} + Q_{evap}) - Q_{conv}, \tag{8}$$

where $H_0 = m_0 c_{,\ell} T_0$ is the total enthalpy of a pure liquid cryogen droplet, $H_{1,\ell} = m_{1,\ell} c_{,\ell} T_1$ is the enthalpy of the remaining liquid droplet at time t_1, $H_{1,g} = m_{1,g} c_{,g} T_1$ is the enthalpy of the cryogen vapor at time t_1, $Q_{evap} = m_{1,g} L$ is the heat driven out from the droplet by the evaporation process, where L is the latent heat of vaporization, and $Q_{conv} = \int_0^{t_1} h_d(t) A(t) [T_\infty - T(t)] \, dt$ is the heat transfer between the droplet and atmosphere, where h_d is the heat transfer coefficient at the droplet surface, and T_∞ the ambient temperature.

Expressing the temperature T_1 from the enthalpy balance (Eq. (8)) yields

$$T_1 = \frac{m_0 c_\ell T_0 - (m_0 - m_{1,\ell}) L + \int h_d A [T_\infty - T(t)] \, dt}{m_{1,\ell} c_\ell + (m_0 - m_{1,\ell}) c_g}. \tag{9}$$

The coefficient h_d may then be expressed in terms of the droplet Nusselt number (Nu), which for forced convection acting on a single droplet is defined as

$$Nu = \frac{h_d D}{k_g}. \tag{10}$$

Substituting h_d in Eq. (9) using Eq. (10) yields

$$T_1 = \frac{m_0 c_\ell T_0 - (m_0 - m_{1,\ell}) L + \int Nu k_g \pi D [T_\infty - T(t)] \, dt}{m_{1,\ell} c_\ell + (m_0 - m_{1,\ell}) c_g}, \tag{11}$$

where according to Ranz and Marshall [14], Nu may be expressed by the following correlation

$$Nu = 2 + 0.6 Re_d^{0.5} Pr_g^{0.33}. \tag{12}$$

By successive iterations, Eq. (11) allows one to estimate the average droplet temperature at time t_1 from initial values D_0, V_0, and T_0. Finally, in order to obtain the droplet temperature as a function of distance from the nozzle, $T(z)$, the distance that a single droplet travels in time t_1 is computed by integrating Eq. (7) over time, i.e., $z = \int_0^{t_1} V(t) \, dt$.

4. Results

Fig. 1 shows low and high magnification images of the cryogenic sprays produced by the two straight-tube nozzles (S and L). As seen from the images, the cryogen exits the nozzle in a jet-like fashion, and widens slightly about 50 mm downstream. From the overall spray

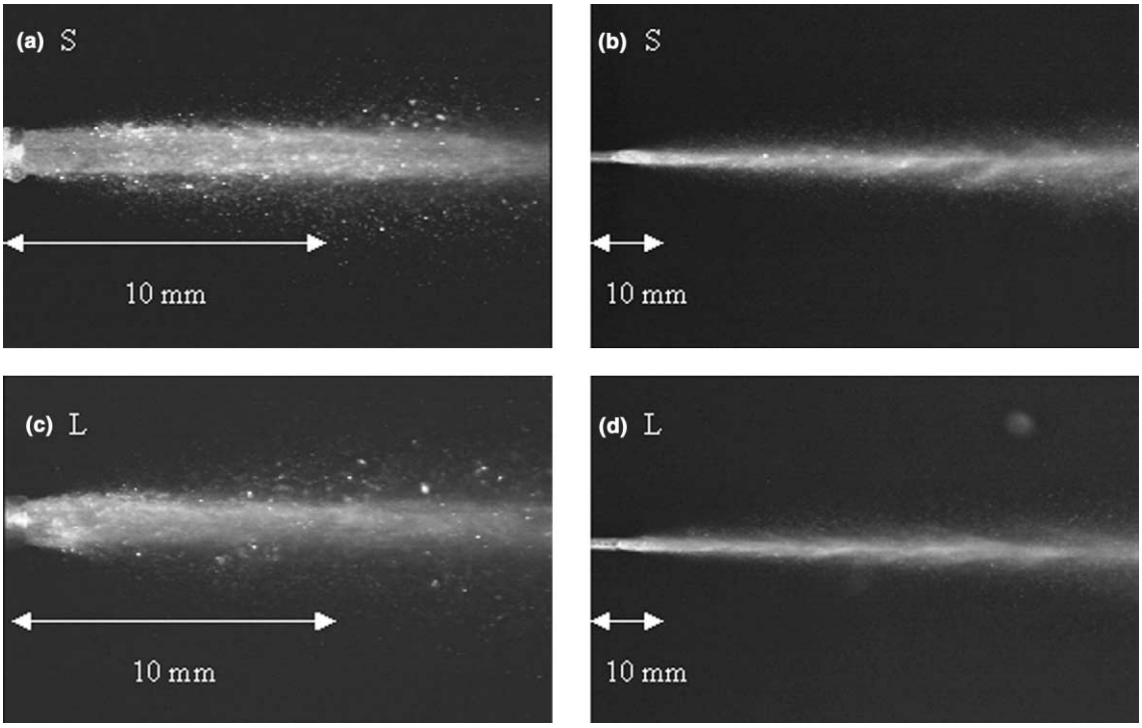

Fig. 1. Photographs of cryogen sprays ejected by S and L nozzles. Images (a) and (c) correspond to the high magnification, i.e., length of field of view is 17 mm. Images (b) and (d) correspond to the low magnification, i.e., length of field of view is 75 mm.

shapes shown in Fig. 1, there seems to be no significant differences in the atomization mechanisms between these nozzles.

Fig. 2 illustrates the strong influence of droplet evaporation in cryogenic sprays. Two measurements of SMD (33 and 51 mm away from the nozzle tip, respectively) for sprays produced by the Scleroplus™ atomizing nozzle are compared with the SMD predicted for water sprays generated by similar straight-tube nozzles [10–12]. As noted, the measured SMD are at least one order of magnitude smaller than those expected for water at a given V. This demonstrates a significant reduction in droplet diameter due to high evaporation rate of cryogenic sprays.

Fig. 3 shows the count number distribution of the droplet axial velocity measured with the PDI for the Scleroplus™ nozzle. Due to space limitations, the closest measurement is taken 33 mm from the nozzle tip. The V at that location is 32 m/s and it diminishes to 19 m/s at 51 mm (as illustrated in Fig. 2). Based on these and other measurement at 89 mm (not shown), V_0 is estimated to 35–40 m/s.

Fig. 4 shows SMD measurements carried out for the S and L nozzles. The solid symbols illustrate the results for the S nozzle, and the hollow ones those obtained for the L nozzle. Error bars represent the estimated standard deviation for each data point. As seen, these measurements show only minimal variation in D between the two nozzles, within the range covered. Unfortunately, it was not possible to obtain measurements closer than 90 mm from the nozzle tip because the spray is very dense – apparently even unbroken jet (see Fig. 1).

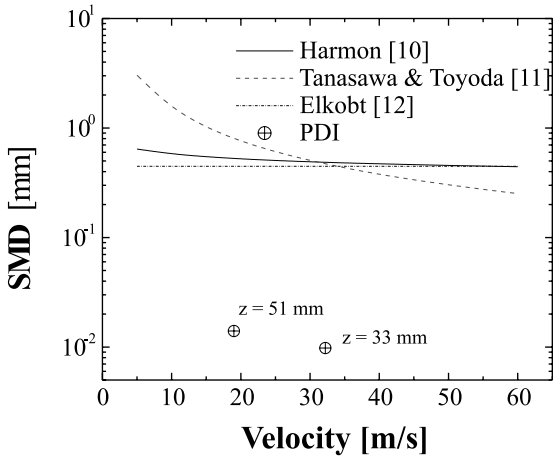

Fig. 2. Sauter mean diameter (SMD) as a function of exit jet velocity according to correlations applicable to water spays [10–12], and preliminary measurements of cryogen sprays using PDI.

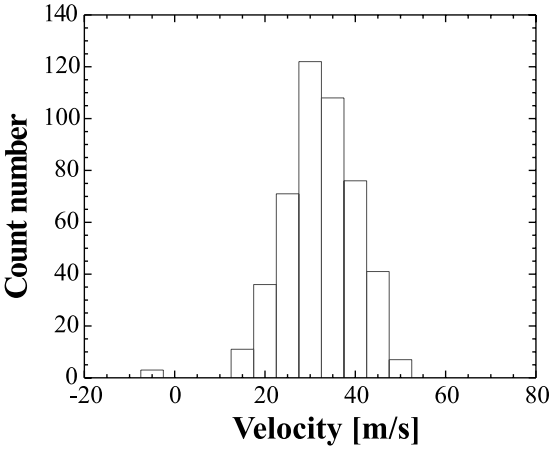

Fig. 3. Droplet velocity distribution obtained from the Scleroplus™ nozzle using PDI at a distance of $z = 33$ mm from the nozzle tip.

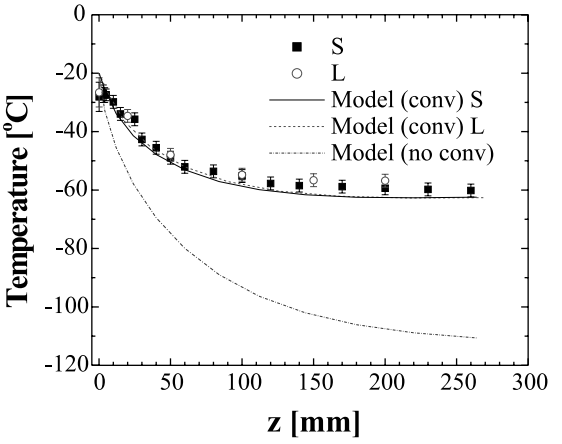

Fig. 5. Measurements and model predictions of the spray temperatures (T) as a function of distance from the nozzle (z). The initial values used in the model are: $V_{0,S} = 60$ m/s, $V_{0,L} = 40$ m/s, $D_0 = 26$ μm, and $T_0 = -20$°C.

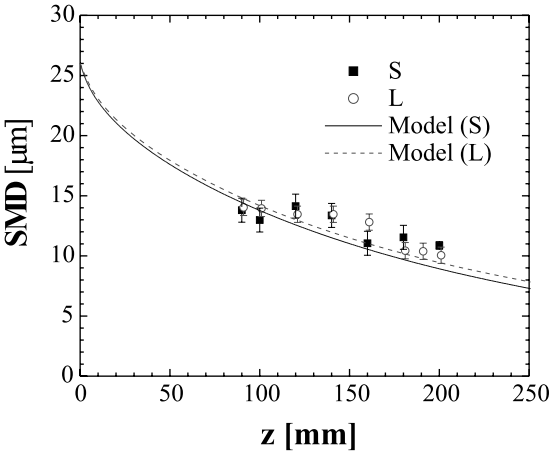

Fig. 4. Sauter mean diameter (SMD) measurements using the EPCS Insitec/Malvern System. The solid and dashed curves represent the SMD predicted by the model for the S and L nozzles, respectively. The initial values used in the model are: $V_{0,S} = 60$ m/s and $V_{0,L} = 40$ m/s, and $D_0 = 26$ μm for both nozzles.

The droplet diameter variation predicted by the single droplet model described in Section 3.3 is also shown by the solid and dashed lines for the S and L nozzles, respectively.

Fig. 5 shows the droplet temperature measurements as a function of z using a bare thermocouple. The solid symbols represent the measurements obtained for the S nozzle, and the hollow ones those obtained for the L nozzle. It is very difficult to obtain a reliable measurement of T for $z < 1.5$ mm, where the temperature readings fluctuate by about 5°C (as indicated by the large error bars in that region). The bold solid and dashed lines represent the computations of $T(z)$ resulting from Eqs. (11) and (12) for the S and L nozzles, respectively. T_0 is a free parameter, which is adjusted until $T(z)$ matches the experimental data best, which is the case for $T_0 = -20$°C. The resulting curves reproduce the experimental data reasonably well up to about $z = 100$ to 150 mm. For $z > 150$ mm, the model predicts somewhat lower temperatures. Computations of $T(z)$ without consideration of the convective term in Eq. (11) are also plotted for comparison (dash–dot line).

The reasonably good match between the proposed model and the experimental data gives a good certainty that $\delta m'/\delta t$ has been appropriately considered. Fig. 6 shows the variation of $\delta m'/\delta t$ as a function of z for

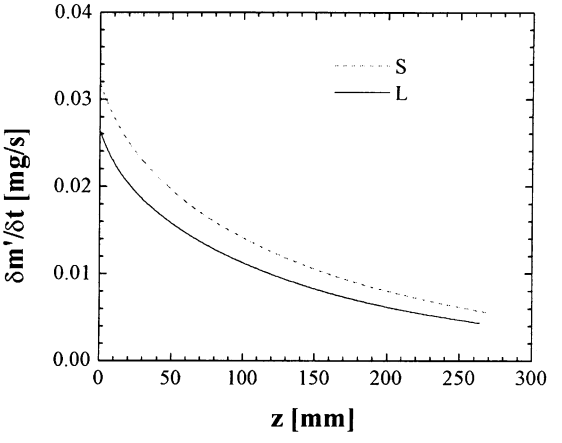

Fig. 6. Variation of $\delta m'/\delta t$ as a function of z (computed from the model using modified Eq. (3)).

sprays generated by S (dashed line) and L (solid line) nozzles, over the same range of distances covered by the temperature measurement ($0 < z < 280$ mm).

5. Discussion

From Fig. 1 it is possible to appreciate that the impact of the nozzle length (L_N) on the overall spray shape is not significant. However, similar photographs have been recently taken of sprays produced by smaller diameter nozzles (D_N ranging from 0.51 to 0.69 mm), showing cone-shape spray forms with apparently finer atomization [22]. In this study, the S and L nozzles are selected as they seem to provide a larger heat transfer coefficient at the skin surface (h_{cryo}) than smaller diameter ones [22] and, therefore, may be more promising for practical applications in dermatology.

As seen in Fig. 4, by adjusting the initial droplet diameter (D_0) to 26 μm, the model describes reasonably well the variation of D with z within the range of 90–200 mm. However, there is not enough evidence to conclude that these curves represent the actual dependence of D for $z < 90$ mm. In particular, the images in Fig. 1 indicate that the sprays are not completely atomized close to the nozzle exit and, therefore, the variation of the SMD in the first few millimeters downstream from the nozzle exit is likely not described properly by this simplified model. Moreover, there seems to be a slight increase in D, or at least a tendency for it to remain invariant within the range of z between 90 and 150 mm. This behavior suggests the possibility of droplet coalescence; a phenomenon observed earlier in liquid and metal spray studies [28,29], and one that is certainly not considered by this single-droplet evaporation model. In fact, a closer look to the two preliminary PDI measurements shown in Fig. 2 also reveals the existence of droplet coalescence, since the value of the SMD increases with increasing distance from the nozzle (from 9.8 μm at 33 mm to 14.0 μm at 51 mm). The presence of this phenomenon may be better studied through more systematic measurements using PDI, which provide simultaneous and localized measurements of D and V. Our recent studies [30,31] indicated a two-fold increase in D within the first 50 mm from the nozzle for 0.7 mm inner diameter nozzles. In addition to droplet coalescence, in the droplet velocity distribution determined using PDI in this study (Fig. 3), it is observed that a small portion of droplets registers a negative axial velocity. This indicates the possibility of particle reentrainment and development of recirculation zones, as reported in earlier spray studies [32,33].

With regard to the values of ρ_ℓ and μ_ℓ used in the computation of V_0 based on Eq. (6), it is possible that the effect of temperature on μ_ℓ is large, as it is for many fluids, especially for the difference in the temperatures of interest. However, the dependence of V_0 on μ_ℓ is practically negligible, since it varies inversely proportional to $\mu_\ell^{-0.125}$ (see Eq. (6)). As an example, for water, a variation in temperature between 0°C and 50°C affects μ_ℓ by a factor of 3.3, which would affect V_0 by only 14%. Such variation is acceptable for the objectives of the present study. Moreover, the model curves for $D(z)$ and $T(z)$ do not depend on μ_ℓ, which makes the value of μ_ℓ even less critical for this study.

From Eq. (6), V_0 was calculated to be 48 m/s for the Scleroplus™ nozzle, which is reasonably close to the value determined from PDI measurements (35–40 m/s). This suggests that Eq. (6) can provide reasonable estimates of the exit velocities (V_0) for the S and L nozzles, which were estimated to be 65 and 44 m/s, respectively. The small discrepancies in the magnitudes of V_0 between PDI measurements and those computed from Eq. (6) may be due to various effects. On one hand, the decrease of V as a function of z for the first 33 mm from the nozzle is not quantified with PDI, so the uncertainty of the extrapolation to obtain V_0 is rather large. On the other hand, computations of V_0 using Eq. (6) do not consider the pressure drops along the hose and solenoid valve. If these pressure drops were considered, lower values of V_0 would result, closer to the values extrapolated from the PDI measurements. Therefore, V_0 values of 60 and 40 m/s were chosen as the input to the model for the S and L nozzles, respectively.

If a significant evaporation upstream of the nozzle tip took place, a two-phase flow, and even supercritical conditions within the nozzle could be met. The appearance of these phenomena could have a large impact on flow dynamics and cryogen atomization process. In Appendix A, theoretical calculations are presented, which suggest that evaporation taking place within the two nozzles is small. This is supported further by the relatively small discrepancies between the predicted values of V_0 and PDI results for both nozzles. Based on this, it is reasonable to conclude that within a reasonable margin of error, the value of V_0 may be estimated from Eq. (6). Moreover, since we have found that its influence on the evolution of D and T is minimal, the selection of this parameter becomes non-critical.

In addition to the small differences in the overall spray shapes pointed out above, the small differences in the modeled D, T and $\delta m'/\delta t$ between the S and L nozzle, also indicate that the effect of nozzle length (L_N) in the spray characteristics is minimal. However, these differences are consistent with the slightly higher velocity at which droplets are ejected from the shorter nozzle, due to the lesser resistance imposed by to the liquid cryogen as it flows within the nozzle. Faster moving droplets are exposed to larger drag forces, which enhance disintegration into smaller ones. Smaller droplets, in turn, have a larger volume-to-surface ratio, which

enhances the evaporation rate and, thus, causes them to cool faster.

Despite the use of dry air to eliminate most of the moisture during temperature measurements, some signs of water condensation and frost formation on the thermocouple were noticed, particularly for $z \geqslant 150$ mm. Upon the appearance of water condensate or frost, an increase in thermocouple reading due to release of the latent heat was detected. For this reason, T_0 has been adjusted in the proposed model to fit best the range of $10 < z < 100$ mm. Notice that the chosen value of T_0 (−20°C) is somewhat higher than suggested by simple extrapolation of the experimental data trend to $z = 0$ (about −26°C).

As demonstrated by Fig. 5, if convective effects are not included in the model, it predicts a much faster decrease of the average droplet temperature than evidenced by the experimental data. This indicates that, while droplets cool by releasing its latent heat of vaporization, the higher temperature of the surrounding air, as well as the drag force exerted on the moving droplets, transfer a significant amount of heat back to the droplets, thus considerably affecting their temperature and, consequently, the diameter evolution.

The values for the three parameters: D_0, V_0 and T_0, were selected primarily based on the best fit to the experimental data in the region where our single-droplet model seems to be applicable. Clearly, since this model does not consider phenomena such as droplet coalescence and recirculation, these values may not necessarily match the actual values of the corresponding variables at nozzles exit. This is true in particular for D_0, which according to the model, should have its highest value at $z = 0$, and in reality, it does not. Since the impact of V_0 on both $D(z)$ and $T(z)$ is small, as mentioned before, this means effectively fitting two free parameters (D_0 and T_0), whereas their experimental determination can provide only vague indication of real physical values.

6. Conclusions

1. A single-droplet model, incorporating the D^2-law, droplet deceleration term, and convective heat transfer into a phase-change heat transfer balance, adequately describes the mean droplet size and temperature evolution of cryogenic sprays produced by the two straight-tube nozzles under study.
2. The experimental data indicate an extended region of droplet coalescence and recirculation near the nozzle tip. Since our model does not include these effects, its validity is restricted to 90–200 mm from the nozzle.
3. Both the experimental results and the model indicate a minor influence of the nozzle length on the cryogen spray droplet evolution.
4. Of the three parameters of the model (D_0, V_0 and T_0), V_0 has the least influence on the cryogen droplet evolution, and can be adequately estimated from theoretical considerations. The other two parameters (D_0 and T_0) need to be fitted to the experimental data in the region where the single-droplet model is applicable. The success of the developed model in reproducing the experimental data represents an additional tool to determine the evaporation rate of cryogenic sprays.

Acknowledgements

The authors wish to acknowledge financial support from the Whitaker Foundation, equipment donation and Grant (No. 482560-59109 to EJL and JSN) from Candela Corp., and funding from the Institute of Arthritis and Musculoskeletal and Skin Diseases, research grant awarded at the National Institutes of Health to JSN (AR43419). Also, we acknowledge Institutional support from the Department of Energy, Office of Naval Research, National Institutes of Health and the Beckman Laser Institute and Medical Clinic Endowment. BM was supported in part by the Slovenian Ministry of Science and Technology.

Appendix A

According to Lockhart and Martinelli [34], the void fraction (α) in a two-phase flow along a tube can be expressed as:

$$\alpha = \left[1 + 0.28\left(\frac{\rho_v}{\rho_\ell}\right)^{0.36}\left(\frac{\mu_\ell}{\mu_v}\right)^{0.07}\left(\frac{1-x}{x}\right)^{0.64}\right]^{-1}, \quad \text{(A.1)}$$

where ρ_v is vapor density, ρ_ℓ is liquid density, μ_v is vapor dynamic viscosity, μ_ℓ is liquid dynamic viscosity, and x is mixture quality.

From the phase diagram for HFC-134a, and assuming a complete adiabatic expansion within the nozzle, a mixture quality is estimated of $x = 0.32$.

Substituting the cryogen property values from Table 2 we obtain $\alpha = 0.928$.

By neglecting the gravitational contribution to the pressure drop (the contribution of this component affects the overall pressure drop much less than 1%), as well as compressibility effects [1], the frictional component of the pressure drop along the nozzle is given by:

[1] In the light of the estimated gas phase velocity (j_v) shown below, this simplication may underestimate the computed ΔP. However, since the real value of x appears to be much lower, the compressibility effects may be safely neglected.

$$\Delta P = \phi_{\ell,0}^2 \left[\frac{2 f_{\ell,0} (\delta m_t/\delta t)^2}{\rho_\ell D_N A_N^2} \right] L_N, \tag{A.2}$$

where ϕ is the two-phase multiplier [35]; f is the friction factor; $_{\ell,0}$ denotes that these variables are in relation to the frictional pressure gradient that would result if the liquid flowed alone through the tube at the same total mass flow rate $(\delta m_t/\delta t)$ [35].

The liquid *corrected* two-phase multiplier $(\phi_{\ell,0})$ used in Eq. (A.2) is defined as [35]:

$$\phi_{\ell,0} = \left(\phi_\ell^2 (1-x)^{1.75} \right)^{1/2}, \tag{A.3}$$

where the liquid two-phase multiplier (ϕ_ℓ) is [34]:

$$\phi_\ell = \left(1 + \frac{C}{X} + \frac{1}{X^2} \right). \tag{A.4}$$

Here, X is the Martinelli parameter, which for a two-phase turbulent–turbulent flow is given by [35]:

$$X = \left(\frac{\rho_v}{\rho_\ell} \right)^{0.5} \left(\frac{\mu_\ell}{\mu_v} \right)^{0.125} \left(\frac{1-x}{x} \right)^{0.875}. \tag{A.5}$$

The *corrected* liquid friction factor may be defined by Blasius as: $f_{\ell,0} = 0.079 Re_N^{-0.25}$.

Considering that the total available pressure (ΔP) is 6.7 bar, Eq. (A.2) can be solved for $\delta m_t/\delta t$, and the following value found:

$\delta m_t/\delta t = 10.1$ mg/s.

Given this flow rate, it is possible to estimate the volume fluxes of the vapor and liquid phases through the tube (j_v and j_ℓ), i.e., the velocity that each phase would have if it flowed at its specific mass flow rate, which is given by the following equations:

$$j_v = \frac{(\delta m_t/\delta t) x}{\rho_v A_N}, \tag{A.6}$$

$$j_\ell = \frac{(\delta m_t/\delta t)(1-x)}{\rho_\ell A_N}, \tag{A.7}$$

where the following values for j_v and j_ℓ are found, respectively:

$j_v = 417$ m/s,
$j_\ell = 3.8$ m/s.

Assuming that our droplet velocity measurements are mostly dictated by j_ℓ, this computed value is much lower than that estimated in Section 4.

If we now work our way backwards and establish as a fixed parameter $j_\ell = 40$ m/s (based on PDI and theoretical calculations presented in Section 4), Eqs. (A.2) and (A.7) may now be solved simultaneously to compute $(\delta m_t/\delta t)$ and x. By doing so, the following values are obtained:

$\delta m_t/\delta t = 71.5$ mg/s,
$x = 0.003$.

Based on these estimations, it is concluded that the evaporation within the nozzle is quite small – significantly less (by 99%) than that expected from a full adiabatic expansion ($x = 0.32$).

References

[1] J.S. Nelson, T.E. Milner, B. Anvari, B.S. Tanenbaum, S. Kimel, L.O. Svaasand, S.L. Jacques, Dynamic epidermal cooling during pulsed laser treatment of port wine stain. A new methodology with preliminary clinical evaluation, Arch. Dermatol. 131 (1995) 695–700.

[2] J.H. Torres, J.S. Nelson, B.S. Tanenbaum, T.E. Milner, et al., Estimation of internal skin temperatures in response to cryogen spray cooling: Implications for laser therapy of port wine stains, IEEE J. Selected Topics Quantum Electron. 5 (1999) 1058–1066.

[3] G.B. Altshuler, H.H. Zenzie, A.V. Erofeev, M.Z. Smirnov, R.R. Anderson, C. Dierickx, Contact cooling of the skin, Phys. Med. Biol. 44 (1999) 1003–1023.

[4] J.S. Nelson, T.E. Milner, B. Anvari, B.S. Tanenbaum, et al., Dynamic epidermal cooling in conjunction with laser-induced photothermolysis of port wine stain blood vessels, Lasers Surg. Med. 19 (1996) 224–229.

[5] S.A. May, Laser technology for hair removal, in: Proceedings of the LEOS '97 10th Annual Meeting IEEE Lasers and Electro-Optics Society, San Francisco, CA, November 1997.

[6] C.J. Chang, J.S. Nelson, Cryogen spray cooling and higher fluence pulsed dye laser treatment improve port-wine stain clearance while minimizing epidermal damage, Dermatol. Surg. 25 (1999) 767–772.

[7] B. Anvari, B.S. Tanenbaum, T.E. Milner, S. Kimel, et al., A theoretical study of the thermal response of skin to cryogen spray cooling and pulsed laser irradiation – implications for treatment of port wine stain birthmarks, Phys. Med. Biol. 40 (1995) 1451–1465.

[8] B. Anvari, B.S. Tanenbaum, T.E. Milner, K. Tang, et al., Spatially selective photocoagulation of biological tissues – feasibility study utilizing cryogen spray cooling, Appl. Opt. 35 (1996) 3314–3320.

[9] W. Verkruysse, B. Majaron, B.S. Tanenbaum, J.S. Nelson, Optimal cryogen spray cooling parameters for pulsed laser treatment of port wine stains, Lasers Surg. Med. 27 (2000) 165–170.

[10] D.B. Harmon, J. Franklin Inst. 259 (1955) 519.

[11] Y. Tanasawa, S. Toyoda, On the atomization of a liquid jet issuing from a cylindrical nozzle, Technical Report of Tohoku University N19-2, Japan, 1955, p. 135.

[12] M.M. Elkobt, Fuel atomization for spray modeling, Prog. Energy Combust. Sci. 8 (1982) 61–91.

[13] G.L. Hubbard, V.E. Denny, A.F. Mills, Int. J. Heat Mass Transfer 16 (1973) 1003–1008.

[14] W.E. Ranz, W.R. Marshall, Evaporation from drops, Chem. Eng. Prog. 48 Part I, 141–146, Part II, 173–180 (1952).

[15] R.D. Ingebo, Effect of gas mass flux on cryogenic liquid jet breakup, paper presented at the Space Cryogenics Workshop, Cleveland OH, June 1991.
[16] R.D. Ingebo, Gas property effects on dropsize of simulated fuel sprays, J. Propulsion 7 (1991) 467–472.
[17] R.D. Ingebo, Effect of vaporization on cryogenic spray dropsize measurement, NASA Technical Memorandum 105909, in: Proceedings of the 31st Aerospace Sciences Meeting and Exhibit by the AIAA, SAE, Reno, NV, 1993.
[18] R.D. Ingebo, Atomizing-gas temperature effect on cryogenic-spray dropsize, NASA Technical Memorandum 106106, in: Proceedings of the 29th Joint Propulsion Conference and Exhibit by the AIAA, SAE, ASME, and ASEE, Monterey, CA, 1993.
[19] R.D. Ingebo, Characteristics of vaporizing cryogenic sprays for rocket combustion modeling, NASA Technical Memorandum 106615.4004966696, 1994.
[20] R.D. Ingebo, Cryogenic and simulated fuel jet breakup in argon, helium and nitrogen gas flows, NASA Technical Memorandum 106923, in: Proceedings of the 31st Joint Propulsion Conference cosponsored by the AIAA, SAE, ASME and ASEE, San Diego, CA, 1995.
[21] K.A. Estes, I. Mudawar, Correlation of Sauter mean diameter and critical heat flux for spray cooling of small surfaces, Int. J. Heat Mass Transfer 38 (1995) 2985–2996.
[22] W. Verkruysse, B. Majaron, G. Aguilar, J.S. Nelson, L.O. Svaasand, Dynamics of cryogen deposition relative to heat extraction rate during cryogen spray cooling, Proceedings SPIE 3907, San Jose CA, 2000, pp. 37–58.
[23] A.H. Lefevbre, Atomization and Sprays, first ed., Taylor & Francis, New York, 1989, p. 309.
[24] Y. Zhou, S. Lee, V.G. McDonell, G.S. Samuelsen, R.L. Kozarek, E.J. Lavernia, Size distribution of spray atomized aluminium alloy powders produced during linear atomization, Mater. Sci. Technol. 15 (1999) 226–234.
[25] Y. Zhou, S. Lee, V.G. McDonell, G.S. Samuelsen, R.L. Kozarek, E.J. Lavernia, Influence of operating variables on average droplet size during linear atomization, Atomization and Sprays 7 (1997) 339–358.
[26] G.A.E. Godsave, Studies of the combustion of drops in fuel spray-the burning of single drops of fuel, in: Proceedings of the Fourth Symposium (International) of Combustion, Williams & Wilkins, Baltimore, 1953, pp. 818–830.
[27] DuPont web page: http://www.dupont.com/dymel/products/pharm.html.
[28] M. Orme, Experiments on droplet collisions bounce coalescence and disruption, Prog. Energy Combust. Sci. 23 (1997) 65–79.
[29] R. Nishitani, A. Kasuya, Y. Nishina, Insitu STM observation of coalescence of metal particles in liquid, Zeitschrift fur Physik D – Atoms, Molecules Clusters 26 (1993) S42–S44.
[30] G. Aguilar, B. Majaron, W. Verkruysse, J.S. Nelson, E.J. Lavernia, Characterization of cryogenic spray nozzles with application to skin cooling, in: Proceedings of the ASME–IMECE 2000, Fluids Engineering Division, FED, vol. 253, 2000, pp. 189–197.
[31] G. Aguilar, B. Majaron, K. Pope, L.O. Svaasand, E.J. Lavernia, J.S. Nelson, Influence of nozzle-to-skin distance in cryogen spray cooling for dermatologic laser surgery, Lasers Med. Surg. 28 (2001) 113–120.
[32] A. Li, G. Ahmadi, M.A. Gaynes, R.G. Bayer, Aerosol particle deposition in a recirculation region, J. Adhesion 51 (1995) 87–103.
[33] J.P. Delplanque, E.J. Lavernia, R.H. Rangel, Numerical investigation of multi-phase flow induced porosity formation in spray-deposited materials, Int. J. Non-Equilibrium Process. 10 (1997) 185–199.
[34] R.W. Lockhart, R.C. Martinelli, Proposed correlation of data for isothermal two-phase, two-component flow in pipes, Chem. Eng. Prog. 45 (1949) 39–48.
[35] V.P. Carey, Liquid–Vapor Phase-Change Phenomena, first ed., Hemisphere, USA, 1992, p. 399.